Electronic spectroscopy and electronic structure of diatomic CrC

Dale J. Brugh,[1,a)] Michael D. Morse,[1,b)] Apostolos Kalemos,[2] and Aristides Mavridis[2]
[1]*Department of Chemistry, University of Utah, Salt Lake City, Utah 84112, USA*
[2]*Department of Chemistry, Laboratory of Physical Chemistry, National and Kapodistrian University of Athens, P.O. Box 64004, Zografou, Athens 157 10, Greece*

(Received 26 March 2010; accepted 1 June 2010; published online 20 July 2010)

Optical spectra of jet-cooled diatomic CrC have been recorded in the near infrared region using resonant two-photon ionization spectroscopy combined with mass-selective detection of the resulting ions. Several weak transitions have been observed, along with one relatively strong band near 842 nm. Rotational resolution and analysis of this band confirms that the ground state is of $^3\Sigma^-$ symmetry. *Ab initio* calculations have been performed that demonstrate that the ground state is highly multiconfigurational in nature, with a leading configuration of $1\sigma^2 2\sigma^2 1\pi^4 1\delta^2$ for the ten valence electrons. From the rotational analysis of the 842 nm $^3\Sigma^- \leftarrow X\ ^3\Sigma^-$ band, the derived spectroscopic constants of the ground and excited states for $^{52}Cr^{12}C$ are $B_0''=0.659\ 97(49)$, $\lambda_0''=6.74(24)$, $\gamma_0''=-0.066(20)$, $T_0=11\ 870.7660(65)$, $B'=0.608\ 29(39)$, $\lambda'=7.11(24)$, and $\gamma'=0.144(17)$ cm^{-1}. Here and throughout this article, 1σ error limits are reported in parentheses. These rotational constants may be inverted to provide the bond lengths in the ground and excited states, $r_0''=1.6188(6)$ Å and $r'=1.6861(5)$ Å, respectively. *Ab initio* calculations show that the upper state is the third state of $^3\Sigma^-$ symmetry. © *2010 American Institute of Physics*. [doi:10.1063/1.3456178]

I. INTRODUCTION

The electronic structure and chemical bonding of the diatomic transition metal carbides are of considerable current interest, owing to the importance of the metal-carbon bond in homogeneous and heterogeneous catalysis, organometallic chemistry, and biological processes. To obtain insight into the organometallic radicals that are intermediates in these processes, we have been investigating the spectra of small organometallic radicals, including the simplest of these species, the diatomic transition metal carbides. The open *d*-subshell transition metal carbides are electronically complicated, often having tens of electronic states lying within 1–2 eV of the ground state.[1] As a result, the accurate prediction of the ground and low-lying electronic states of these species provides a serious challenge to quantum chemistry. The existence of such a large density of states also makes the spectroscopic study of such species difficult, owing to the complicated spectra that are often obtained.

Published spectroscopic data on the 3*d* series of transition metal carbides, MC, are limited to the VC,[2,3] FeC,[4–13] CoC,[2,14–17] and NiC molecules,[16,18] for which the ground states have been identified as $^2\Delta_{3/2}(1\sigma^2 2\sigma^2 1\pi^4 1\delta^1)$, $^3\Delta_3(1\sigma^2 2\sigma^2 3\sigma^1 1\pi^4 1\delta^3)$, $^2\Sigma^+(1\sigma^2 2\sigma^2 3\sigma^1 1\pi^4 1\delta^4)$, and $^1\Sigma^+(1\sigma^2 2\sigma^2 3\sigma^2 1\pi^4 1\delta^4)$, respectively. Here and throughout this paper, only the valence molecular orbitals are listed; these are based primarily on the metal 3*d* and 4*s* and the carbon 2*s* and 2*p* atomic orbitals. In contrast to the spectroscopic work, the entire set of the neutral 3*d*-transition metal carbides, ScC,[19] TiC,[20] VC,[21] CrC,[22] MnC,[23] FeC,[24–26] CoC,[27] NiC,[28] CuC,[29] and ZnC,[30,31] has been investigated by high level *ab initio* calculations.

It is computationally well established that the ground state of CrC is of $^3\Sigma^-$ symmetry with a leading configuration of ~(0.8) $1\sigma^2 2\sigma^2 1\pi^4 1\delta^2$ (see Ref. 22 and references therein). At the best computational level published so far on CrC,[22] the molecule shows some ionic character, with Mulliken charges $Cr^{+0.3}C^{-0.3}$ at the multireference level and a calculated dipole moment $\mu(X\ ^3\Sigma^-)\approx 6.8$ D.

Despite the intense computational interest in the CrC molecule, no spectroscopic results have been reported to date. In this article we report rotationally resolved studies of a $^3\Sigma^- \leftarrow X\ ^3\Sigma^-$ band system near 11 870 cm^{-1}. This confirms the identity of the ground state and provides the first measurement of the CrC bond length. Prompted by the experimental findings, we decided to revisit our previous theoretical work,[22] and to include additional states of $^3A_2$ symmetry that were not considered in Ref. 22. To this end we constructed potential energy curves for the first six states of $^3A_2$ symmetry ($^3\Sigma^-[3]$, $^3\Delta[2]$, $^3\Gamma$) through multireference variational methods.

It can be confusing to report calculations on a diatomic molecule using term symbols that pertain to the C_{2v} subgroup, in this case $^3A_2$. Owing to calculational difficulties associated with the use of non-Abelian point groups, most computational codes are only able to treat $C_{\infty v}$ molecules in the C_{2v} subgroup. Thus, actual calculations are performed in C_{2v}, but examination of the resulting wave functions allows them to be classified properly according to the irreducible representations of the $C_{\infty v}$ point group.

[a)]Present address: Ohio Wesleyan University, 61 S. Sandusky St., Delaware, OH 43015.
[b)]Electronic mail: morse@chem.utah.edu. FAX: (801)-581-8433.

II. EXPERIMENTAL METHODS

Diatomic CrC was produced by pulsed laser ablation (Neodymium: Yttrium aluminum garnet second harmonic, 532 nm) of a Cr disk in the throat of a pulsed supersonic expansion of helium seeded with 3% CH_4 and maintained at a reservoir pressure of 60 psi. Following the point of vaporization, the high pressure gas mixture flowed through a narrow channel (2 mm diameter $\times$ 1.3 cm long) prior to expansion into a large vacuum chamber maintained at a pressure of 1×10^{-4} Torr. The resulting supersonically cooled mixture of reaction products was roughly collimated by passage through a 1 cm diameter skimmer and then entered the ionization region of a Wiley–McLaren reflectron time-of-flight mass spectrometer,[32,33] maintained at a pressure of 1×10^{-6} Torr. In the center of the ion extraction zone, the molecules were exposed to tunable radiation produced by either a dye laser or an optical parametric oscillator-optical parametric amplifier (OPO-OPA) laser that was counterpropagated along the molecular beam axis. Approximately 30 ns after the excitation pulse, the molecules were exposed to the 193 nm (6.42 eV) output of an ArF excimer laser, which crossed the molecular beam axis at right angles. When the molecules were successfully excited by the tunable radiation, absorption of a 193 nm photon led to efficient resonantly enhanced ionization. By monitoring the signal in the mass spectrometer at mass 64, the optical spectrum of $^{52}Cr^{12}C$ was recorded.

Excited state lifetimes were measured by varying the interval between the excitation laser and excimer laser pulses and recording the ion signal as a function of this delay. The resulting curve was fitted to an exponential decay function using the Levenberg–Marquardt algorithm to extract the excited state lifetime.[34] Decay curves were recorded a minimum of four times and were independently fitted. The fitted lifetimes were then averaged, and the standard deviation (1σ) between the fitted values is also reported. For these experiments, the excimer laser was fired at the time corresponding to the greatest density of molecules in the ionization region, and the timing of the tunable excitation laser was varied. By counterpropagating the tunable laser along the molecular beam path, this arrangement permitted long lifetimes to be reliably measured. In contrast, if the two lasers had been arranged so they overlapped and crossed the molecular beam at right angles, the effect of molecules translating out of the ionization region would have limited the measurement capability to short lifetimes only. With the arrangement described here, it has been possible to measure lifetimes that are as long as 100 μs.[35,36]

The rotationally resolved scans were collected using an OPO-OPA laser that first split the second harmonic of a seeded Nd:YAG laser into a signal beam (higher frequency) and an idler beam (lower frequency) using the OPO process. The higher frequency signal beam was then selected and made coaxial with the third harmonic output of the same seeded Nd:YAG laser. A pair of beta-barium borate crystals was then used to amplify the signal beam and simultaneously generate the difference frequency between the third harmonic frequency and the signal frequency. The amplified signal beam was then used to record the rotationally resolved spectrum of CrC in the 11 870 cm^{-1} range. The complementary output radiation, near 16 313 cm^{-1}, was sent into an I_2 fluorescence cell, and this wavelength was calibrated using the iodine atlas of Gerstenkorn and Luc.[37,38]

In separate experiments, this system was operated in a wavelength range in which both of the final output frequencies could be sent into separate iodine cells, and the resulting spectra compared to the iodine atlas of Gerstenkorn and Luc.[37,38] After calibrating both spectra and summing the wavenumbers at each data point, it was determined that the third harmonic of the seeded Nd:YAG laser had a wavenumber of 28 183.594 $\pm$ 0.008 cm^{-1}. By subtracting the wavenumber of the calibrated output radiation near 16 313 cm^{-1} from the wavenumber of the third harmonic radiation (28 183.594 cm^{-1}), it was possible to properly calibrate the spectrum recorded for CrC. As a final step, a correction was made for the Doppler shift experienced by the CrC molecules as they traveled toward the radiation source at the beam velocity of helium (approximately 1.77×10^5 cm/s). This amounted to a correction of +0.07 cm^{-1} for all of the rotational lines observed.

Although we normally expect our calibration to be accurate to better than $\pm$0.01 cm^{-1}, the procedure described above demands that the third harmonic frequency of the Nd:YAG laser be constant from day to day. In measurements conducted 9 months apart, however, we found that the third harmonic had drifted by 0.176 cm^{-1}. Thus, there is an overall measurement uncertainty of this magnitude in our results. The actual error should be less than this, however, because the third harmonic frequency that was used in the calibration of the present data was measured within 5 days of the collection of the rotationally resolved scans. In any case, this error is expected to affect all of the lines systematically, leading to an overall error in the band origin, T_0 and not in the remaining parameters (B_0'', λ_0'', γ_0'', B', λ', γ', r_0'', and r').

III. COMPUTATIONAL METHODS

For the Cr atom the correlation consistent $28s20p12d4f3g2h1i$ basis set of quintuple cardinality of Balabanov and Peterson was used,[39] whereas for the C atom the cc-pV5Z of Dunning was employed.[40] Both sets were generally contracted to $[9s8p6d4f3g2h1i/_{Cr}6s5p4d3f2g1h/_C]$, a total of 244 spherical Gaussians.

The active space, similar to our previous study,[22] consists of ten orbitals correlating to the valence space of both atoms, i.e., $(4s+3d)_{Cr}+(2s+2p)_C$. The distribution of ten valence electrons to ten orbitals gives rise to complete active space self-consistent field (CASSCF) wave functions of 7476 configuration functions (CFs). The order of the valence multireference configuration interaction space (MRCI =CASSCF+single+double replacements) is $\sim400\times10^6$ CFs, reduced to $\sim6.5\times10^6$ CFs through the internal contraction scheme as implemented in the MOLPRO package.[41] The one electron CASSCF orbitals were obtained from an equal-weighted state averaged calculation of 10 $^3A_2$ states. Size nonextensivity errors were ameliorated through the Davidson correction.[42,43] Core subvalence effects of Cr ($3s^23p^6$) and

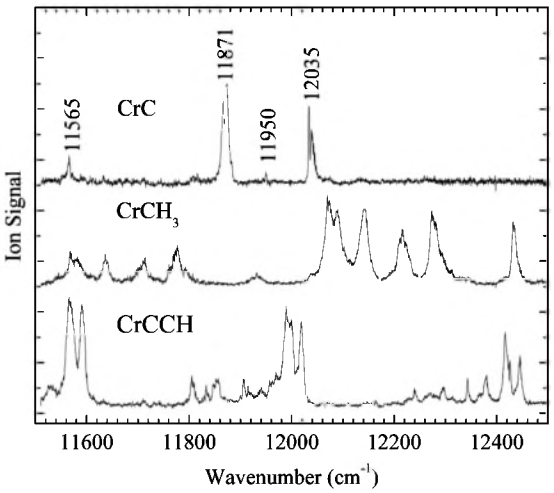

FIG. 1. Vibronically resolved spectra of jet-cooled CrC, $CrCH_3$, and CrCCH produced by laser ablation of chromium metal in a supersonic expansion of 3% CH_4 in helium.

scalar relativistic effects were not taken into account, as these are considered to be of minor importance for the purpose of the present investigation.

For six states, $X\ ^3\Sigma^-$, $1\ ^3\Delta$, $2\ ^3\Sigma^-$, $3\ ^3\Sigma^-$, $2\ ^3\Delta$, and $1\ ^3\Gamma$, we report total energies, common spectroscopic parameters, and dipole moments, which have been calculated as expectation values ($\langle\mu\rangle$) and by the finite field approach (μ_{FF}), with the latter believed to be more reliable.[25]

IV. EXPERIMENTAL AND THEORETICAL RESULTS

A. Low resolution spectrum of CrC

Scans were conducted for spectroscopic transitions in the CrC molecule over the region 11 510–12 550 cm^{-1} and from 12 900–16 190 cm^{-1}. A number of weak features were found in the latter region, but strong features were found deeper in the near infrared. Figure 1 displays the spectra collected for CrC (and for the simultaneously formed $CrCH_3$ and CrCCH molecules) in the 11 500–12 500 cm^{-1} region.

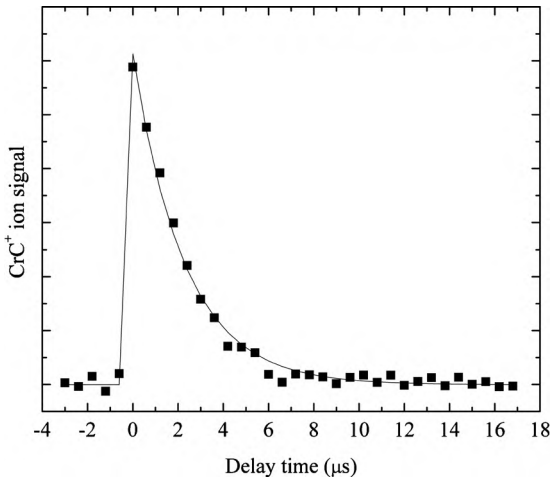

FIG. 2. Excited state decay measurements for the 11 871 cm^{-1} band (data points) and fitted decay curve (solid line). Based on four independent measurements of this decay curve, the upper state lifetime is found to be 2.06 ± 0.17 μs (1σ error limit).

TABLE I. Observed bands of CrC.

Wavenumber (cm^{-1})	Relative intensity	Excited state lifetime (μs) [a]
11 565	Weak	
11 871	Strong, rotationally resolved	2.06(17)
11 950	Very weak	
12 035	Strong	10.9(7)
13 093	Weak	
13 680	Very weak	
13 898	Weak	
13 951	Very weak	
14 386	Weak	
14 668	Weak	
14 705–14 784	Several features, all very weak	
15 068	Very weak	
15 440	Weak	

[a]The value in parentheses provides the 1σ error limit, in units of the last digit reported.

In addition to these three molecules, CrH and a molecule of mass 90 (possibly $^{52}CrC_3H_2$) also have intense transitions in the 11 500–12 500 cm^{-1} region. Table I provides a list of all of the observed vibronic transitions of CrC. Some of these bands, particularly those lying near 13 093, 13 898, 14 668, and 15 440 cm^{-1}, may be part of a vibrational progression. Unfortunately, their intensities are too weak to permit a more detailed investigation.

Excited state lifetimes were measured for the more intense transitions at 11 871, and 12 035 cm^{-1}, using the methods described above. The quality of one of the lifetime fits is illustrated in Fig. 2, and the resulting lifetimes are reported in Table I.

B. Rotationally resolved spectra

Attempts were made to rotationally resolve the bands near 11 871 and 12 035 cm^{-1}, but success was only achieved for the 11 871 cm^{-1} band. The rotationally resolved spectrum displayed in Fig. 3 shows the structure of the 11 871 cm^{-1} band in detail.

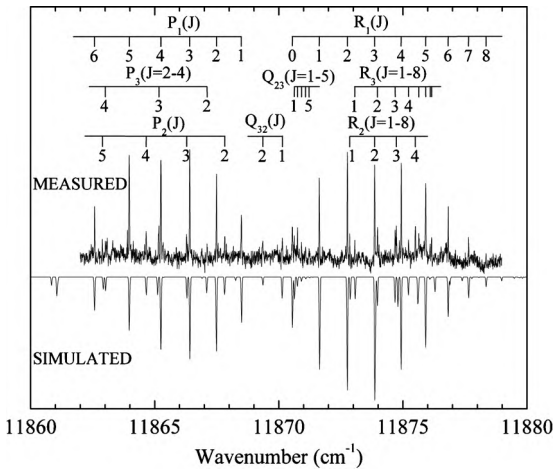

FIG. 3. Rotationally resolved spectrum of the 11 871 cm^{-1} band of $^{52}Cr^{12}C$, with rotational lines identified.

TABLE II. Rotational lines and fitted parameters of 11 871 cm^{-1} $^3\Sigma^- \leftarrow X\ ^3\Sigma^-$ band of $^{52}Cr^{12}C$.

Line	Wavenumber	Line	Wavenumber	Line	Wavenumber
$P_1(1)$	11 868.7367(−84)	$R_1(7)$	11 877.9201(240)	$R_3(3)$	11 874.9334(−36)
$P_1(2)$	11 867.7339(71)	$R_1(8)$	11 878.5971(−193)	$R_3(4)$	11 875.4753(−57)
$P_1(3)$	11 866.6547(14)	$P_2(2)$	11 868.0713(146)	$R_3(7)$	11 876.3426(69)
$P_1(4)$	11 865.4945(53)	$P_2(3)$	11 866.5319(19)	$R_3(8)$	11 876.4010(64)
$P_1(5)$	11 864.2199(53)	$P_2(4)$	11 864.8999(0)	$Q_{32}(1)$	11 870.8719(26)
$P_1(6)$	11 862.8249(35)	$P_2(5)$	11 863.1363(−302)	$Q_{32}(2)$	11 871.0010(54)
$R_1(0)$	11 870.7918(−74)	$R_2(1)$	11 873.1051(−246)	$Q_{32}(3)$	11 871.1613(38)
$R_1(1)$	11 871.8768(−122)	$R_2(4)$	11 875.8877(387))	$Q_{32}(4)$	11 871.3239(−69)
$R_1(2)$	11 873.0094(47)	$P_3(2)$	11 867.3596(175)	$Q_{32}(5)$	11 871.4745(−183)
$R_1(3)$	11 874.1084(−20)	$P_3(3)$	11 865.4108(485)	$Q_{23}(1)$	11 870.3905(35)
$R_1(4)$	11 875.1801(75)	$P_3(4)$	11 863.2650(−12)	$Q_{23}(2)$	11 869.5907(−117)
$R_1(5)$	11 876.1647(−22)	$R_3(1)$	11 873.3116(−143)	$Q_{23}(4)$	11 867.1457(−91)
$R_1(6)$	11 877.0714(−64)	$R_3(2)$	11 874.2238(−60)	$Q_{23}(5)$	11 865.5732(−190)

Fitted parameters (all in cm^{-1}, except for r_0'' and r')[b]

T_0=11 870.7660(65)

B_0''=0.659 97(49) B'=0.608 29(39)

λ_0''=6.743(239) λ'=7.108(235)

γ_0''=−0.0660(203) γ'=0.1439(165)

r_0''=1.618 75(60) Å r'=1.686 13(54) Å

Correlation matrix

	B_0''	λ_0''	γ_0''	T_0	B'	λ'	γ'
B_0''	1.000						
λ_0''	0.241	1.000					
γ_0''	−0.213	−0.995	1.000				
T_0	0.417	0.783	−0.776	1.000			
B'	0.956	0.227	−0.202	0.296	1.000		
λ'	0.242	1.000	−0.995	0.785	0.229	1.000	
γ'	−0.212	−0.993	0.998	−0.766	−0.198	−0.992	1.000

[a]Following the wavenumber of each line, the residual (measured–calculated) is provided in units of 0.0001 cm^{-1}.

[b]1σ error limits are provided in parentheses following each value, in units of the last reported digits.

The band is dominated by intense lines belonging to an R- and a P-branch. Attempts to fit these line positions to a simple BJ(J+1) dependence in the upper and lower states, however, fail miserably, leading to errors of more than 0.1 cm^{-1} in more than half of the lines. The key to assigning the band was paying attention to the weak features in the spectrum, which arise from the spin splitting of levels in the X $^3\Sigma^-$ state as well as in the upper $^3\Sigma^-$ state. In both states, there is a significant spin-orbit interaction with other states, causing the $^3\Sigma^-$ state to split into $\Omega=0^+$ and $\Omega=\pm1$ levels. This is primarily due to the spin-orbit interaction with the $^1\Sigma^+$ state that derives from the same configuration as the $^3\Sigma^-$ state. Taking into account that the X $^3\Sigma^-$ state derives primarily from the $1\sigma^2 2\sigma^2 1\pi^4 1\delta^2$ configuration, methods described by Lefebvre-Brion and Field[44] and originally suggested by Ishiguro and Kobori[45] show that the matrix element connecting the X $^3\Sigma^-$ state with the isoconfigurational $^1\Sigma^+$ state is given by $2\zeta_{3d}$(Cr), which is approximately 486 cm^{-1}. The large magnitude of this off-diagonal element causes the $\Omega=0^+$ component of the ground state to be pushed to lower energies. Nevertheless, the $\Omega=\pm1$ levels, which are split into e/f components, remain weakly populated in the supersonic beam, and these are responsible for the weaker features in the spectrum.

The spectrum was assigned, fitted, and simulated using PGOPHER, a freely available general purpose program for simulating and fitting rotational, vibrational, and electronic spectra.[46] The lines were fitted according to a $B\hat{\mathbf{N}}^2$ form of the rotational Hamiltonian,

$$\hat{H} = B_v\hat{\mathbf{N}}^2 + \gamma_v\hat{\mathbf{N}}\cdot\hat{\mathbf{S}} + 2/3\lambda_v(3\hat{S}_z^{\ 2} - \hat{\mathbf{S}}^2),$$

for both the upper and lower states. For such a system, each N value greater than 0 (or J value greater than 0) leads to three energy levels, which are designated as F_1, F_2, and F_3. In agreement with the conventions described by Herzberg,[47] these correspond to the cases J=N+1 (F_1, *e* parity), J=N (F_2, *f* parity), and J=N−1 (F_3, *e* parity). For low J-values, the F_1 levels also correspond to the $\Omega=0^+$ levels while the F_2 and F_3 levels correspond to the $\Omega=\pm1$ levels of *f* and *e* parity, respectively. The strong branches observed in the spectrum are the R_1 and P_1 branches, labeled according to the value of J″ in Fig. 3. The weaker lines belong to the R_2, P_2, and Q_{32} branches, which originate from the F_2'' levels of the lower state, and to the R_3, P_3, and Q_{23} branches, which originate from the F_3'' levels. Table II provides a list of all measured line positions, with assignments given in terms of J″. Residuals in the least-squares fit are provided in paren-

TABLE III. Total energies $E_e(E_h)$, bond lengths $r_e/r_0(Å)$, dissociation energies $D_e(kcal/mol)$, harmonic and anharmonic frequencies ω_e, $\omega_e x_e(cm^{-1})$, vibrational-rotational coupling constants $\alpha_e(cm^{-1})$, zero point energies ZPE(cm^{-1}), dipole moments $\mu_e(D)$, and energy separations $T_0(cm^{-1})$ of $^{52}Cr^{12}C$ at the MRCI(MRCI+Q) level of theory.

State	$-E_e$	r_e/r_0	D_e [a]	ω_e	$\omega_e x_e$	$\alpha_e \times 10^3$	ZPE	$\langle\mu\rangle/\mu_{FF}$ [b]	T_0
$X\ ^3\Sigma^-$	1081.345 31	1.639/1.645	87.5	801.4	6.50	7.69	399.1	6.70/6.78	0.0
	(1081.372 3)	(1.632/1.640)	(95)	(833)	(39.5)	(7.8)	(407.4)	/(6.68)	(0.0)
Expt.[c]		/1.61875(60)							
$1\ ^3\Delta$	1081.332 71	1.620/1.621	86.0	879.8	8.17	6.50	437.7	2.27/2.65	2 804
	(1081.351 1)	(1.622/1.624)	(87)	(879)	(8.0)	(6.1)	(437.9)	/(2.75)	(4 683)
$2\ ^3\Sigma^-$	1081.311 79	1.802/1.807	72.8	592.5	7.62	1.91	292.9	1.64/1.98	7 251
	(1081.329 1)	(1.797/1.801)	(73)	(583)	(13.3)	(2.68)	(289.0)	/(2.11)	(9 363)
$3\ ^3\Sigma^-$	1081.294 10	1.673/1.682	61.7	922.1	18.48	7.54	456.1	1.64/1.78	11 296
	(1081.314 6)	(1.674/1.684)	(64)	(933)	(11.6)	(8.0)	(468.2)	/(1.45)	(12 724)
Expt.[c]		/1.68613(54)							11 870.7660(65)
$2\ ^3\Delta$	1081.268 83	1.786/1.792	45.9	697.8	11.86	4.30	344.4	1.77/2.42	16 731
	(1081.291 9)	(1.755/1.761)	(50)	(713)	(4.72)	(4.8)	(354.8)	/(2.30)	(17 593)
$1\ ^3\Gamma$	1081.267 41	1.652/1.656	77.7	772.6	−73.58	6.14	414.4	1.52/2.12	17 112
	(1081.287 4)	(1.656/1.661)	(82)	(883)	(−10.8)	(4.9)	(446.2)	/(2.32)	(18 672)

[a]With respect to the adiabatic atoms; see text.
[b]$\langle\mu\rangle$ calculated as an expectation value, μ_{FF} by the finite field approach; field strengths $10^{-5}-10^{-4}$ a.u.
[c]Present work.

theses after each line position, in units of 0.0001 cm^{-1}.

Also given in Table II are the values of the fitted spectroscopic constants, B_0'', λ_0'', γ_0'' for the ground state and T_0, B', λ', and γ' for the excited state, along with their 1σ error limits (in parentheses, in units of the last reported digits). In this fit, 39 measured lines are reproduced with a rms error of 0.015 cm^{-1}. It should be noted, however (see the correlation matrix reported in Table II), that some of the spectroscopic constants are highly correlated (λ_0'' and λ', for example), so that despite the quality of the fit, these parameters remain imperfectly determined. In the case of λ_0'' and λ', the difference of these parameters is well known, but the individual values are not known to the precision suggested by the error limits quoted. Finally, the B-values have been inverted to give the vibrationally averaged bond lengths in the ground and excited states, as listed in Table II.

C. *Ab initio* results and discussion

Table III collects all calculated parameters for the $X\ ^3\Sigma^-$, $1\ ^3\Delta$, $2\ ^3\Sigma^-$, $3\ ^3\Sigma^-$, $2\ ^3\Delta$, and $1\ ^3\Gamma$ states pertaining to the potential energy curves shown in Fig. 4; for ease of comparison, relevant experimental results are also included. In our previous theoretical work[22] only two states of $^3A_2$ symmetry were reported, $X\ ^3\Sigma^-$ and $1\ ^3\Delta$, with nearly identical results as in the present study.

From the lowest state channel, $Cr(^7S;4s^13d^5)+C(^3P;2s^22p^2)$, only $^{5,7,9}\Sigma^-$ and $^{5,7,9}\Pi$ states can be obtained. The six triplets considered here correlate adiabatically to $Cr(^5S;4s^13d^5)+C(^3P;2s^22p^2)$ [$X\ ^3\Sigma^-$], $Cr(^5D;4s^23d^4)+C(^3P;2s^22p^2)$ [$1\ ^3\Delta$, $2\ ^3\Sigma^-$, $3\ ^3\Sigma^-$, and $2\ ^3\Delta$], and $Cr(^5G;4s^13d^5)+C(^3P;2s^22p^2)$ [$1\ ^3\Gamma$], where the ^5S, ^5D, and ^5G terms are located experimentally[48] (theoretically=MRCI+Q) at 7593.16 (7006), 8090.21 (8572), and 20 521.44(21 717) cm^{-1}, respectively, above the ground ^7S term of Cr.

The leading equilibrium MRCI configurations of the $X\ ^3\Sigma^-$, $2\ ^3\Sigma^-$, and $3\ ^3\Sigma^-$ states and corresponding Mulliken populations are as follows (only valence electrons are listed):

$$|X\ ^3\Sigma^-\rangle \approx 0.76|1\sigma^2 2\sigma^2 1\delta_+^1 1\pi_x^2 1\pi_y^2 1\delta_-^1\rangle + 0.20|1\sigma^2 2\sigma^1 3\sigma^1 1\bar{\delta}_+^1 1\pi_x^2 1\pi_y^2 1\delta_-^1\rangle + 0.14|1\sigma^2 2\sigma^1 3\sigma^1 1\delta_+^1 1\pi_x^2 1\pi_y^2 1\bar{\delta}_-^1\rangle + 0.14|1\sigma^2 2\sigma^1 1\bar{\delta}_+^1 4\sigma^1 1\pi_x^2 1\pi_y^2 1\delta_-^1\rangle,$$

$$4s^{0.35}4p_z^{0.14}3d_{z^2}^{1.11}4p_x^{0.04}4p_y^{0.04}3d_{xz}^{1.02}3d_{yz}^{1.02}3d_{x^2-y^2}^{1.0}3d_{xy}^{1.0}/2s^{1.58}2p_z^{0.76}2p_x^{0.92}2p_y^{0.92},$$

$$|2\ ^3\Sigma^-\rangle \approx 0.54|1\sigma^2 2\sigma^1 3\bar{\sigma}^1 1\delta_+^1 1\pi_x^2 1\pi_y^2 1\delta_-^1\rangle - 0.29|1\sigma^2 2\sigma^2 1\delta_+^1 1\pi_x^2 1\pi_y^2 1\delta_-^1\rangle + 0.20|1\sigma^2 2\sigma^1 3\sigma^1 1\bar{\delta}_+^1 1\pi_x^2 1\pi_y^2 1\delta_-^1\rangle,$$

$$4s^{0.91}4p_z^{0.30}3d_{z^2}^{0.31}4p_x^{0.03}4p_y^{0.03}3d_{xz}^{1.08}3d_{yz}^{1.08}3d_{x^2-y^2}^{1.0}3d_{xy}^{1.0}/2s^{1.63}2p_z^{0.81}2p_x^{0.87}2p_y^{0.87},$$

$$|3\,^3\Sigma^-\rangle \approx 0.54|1\sigma^2 2\sigma^1 3\sigma^1 1\bar{\delta}_+^1 1\pi_x^2 1\pi_y^2 1\delta_-^1\rangle + 0.41|1\sigma^2 2\sigma^1 3\sigma^1 1\delta_+^1 1\pi_x^2 1\pi_y^2 1\bar{\delta}_-^1\rangle - 0.28|1\sigma^2 2\sigma^2 1\delta_+^1 1\pi_x^2 1\pi_y^2 1\delta_-^1\rangle,$$

$$4s^{0.84}4p_z^{0.27}3d_{z^2}^{0.70}4p_x^{0.04}4p_y^{0.04}3d_{xz}^{1.0}3d_{yz}^{1.0}3d_{x^2-y^2}^{1.0}3d_{xy}^{1.0}/2s^{1.56}2p_z^{0.59}2p_x^{0.94}2p_y^{0.94}.$$

Observe the severe multireference character of the states above; for instance, the sum $\Sigma_{k=1}^{40}|C_k|^2$, where $\{C_k\}$ are MRCI variational coefficients, is 0.83 for the X $^3\Sigma^-$ state. Overall 0.27, 0.25, and 0.11 e^- are transferred from Cr to the C atom in the X $^3\Sigma^-$, 2 $^3\Sigma^-$, and 3 $^3\Sigma^-$ states, respectively. The bonding in the X-state can be schematically represented by the following valence-bond-Lewis diagram

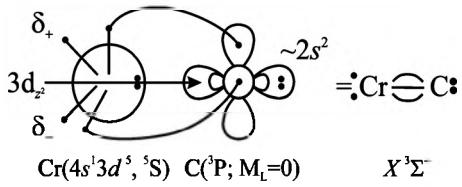

The bonding consists of a σ bond ($2\sigma^2$ distribution) through a transfer of electron density to the empty $2p_z$ C orbital, and two putative π bonds due to the $\alpha\beta-\beta\alpha$ spin coupling of four completely localized electrons, two d_π and two p_π.

The MRCI+Q binding energy with respect to Cr(^{5}S) +C(^{3}P) is calculated to be $D_e(D_0)=95(94)$ kcal/mol, as contrasted to 91.4 kcal/mol of Ref. 22; with respect to the ground state atoms $D_e^0(D_0^0)=95(94)-\Delta E_{MRCI+Q}(^5S\leftarrow{}^7S)=75(74)$ kcal/mol. No corresponding experimental dissociation energy exists in the literature for CrC. It should be mentioned that the potential energy curve of the X $^3\Sigma^-$ state displayed in Fig. 4 fails to open correctly to Cr(^{5}S), instead correlating to Cr(^{5}D), indicating the inherent difficulties of these calculations. The calculated MRCI(+Q) bond length is $r_0=1.645(1.640)$ Å, in fair agreement with the experimental value, the latter being smaller by ~0.02 Å. Certainly the inclusion of the $3s^23p^6$ subvalence electrons of Cr would reduce the bond distance by about 0.01 Å; see Ref. 49. Finally, our recommended dipole moment is $\mu_{FF}=6.7-6.8$ D.

The lack of a really dominant configuration in the MRCI expansion of the 2 $^3\Sigma^-$ and 3 $^3\Sigma^-$ states precludes any discussion concerning their bonding nature. Both states correlate adiabatically to Cr(^{5}D:$4s^23d^4$)+C(^{3}P; $2s^22p^2$), but the 3 $^3\Sigma^-$ state correlates *diabatically* to Cr(^{5}G:$4s^13d^5$) +C(^{3}P; $2s^22p^2$), as evidenced by the Mulliken population analysis and the avoided crossing shown in Fig. 4 near 5 bohr.

The MRCI(+Q) 3 $^3\Sigma^-\leftarrow$ X $^3\Sigma^-$ transition is $T_0=11\,296$ (12 724) cm^{-1}, in relative good agreement with the presently observed experimental transition of 11 870.766 cm^{-1}, thus confirming the experimental assignment of the upper state to a $^3\Sigma^-$ symmetry. Disregarding the MRCI+Q T_0 result as overestimated, we can suggest that the observed transition is vibrationally the 1–0 band, with a calculated $T_{v'v''}=T_{10}=T_e+G_{v'=1}-G_{v''=0}=11\,240+1341-399=12\,182$ cm^{-1}. The calculated r_e/r_0 bond distance of the 3 $^3\Sigma^-$ state is 1.673(1.674)/1.682(1.684) Å in good agreement with the experimentally determined r=1.68613(54) Å.

Recommended dissociation energies [for dissociation to Cr(^{5}D:$4s^23d^4$)+C(^{3}P; $2s^22p^2$)] and dipole moments are $D_e(D_0)=73(72)$, 64(63) kcal/mol and $\mu_{FF}=2.1$, 1.5 D for the 2 $^3\Sigma^-$ and 3 $^3\Sigma^-$ states, respectively; see Table III.

Three more calculated states are of $^3\Delta[2]$ and $^3\Gamma$ symmetry, correlating adiabatically to Cr(^{5}D;$4s^23d^4$) and Cr(^{5}G;$4s^13d^5$)+C(^{3}P; $2s^22p^2$). The main MRCI equilibrium configuration of the $1^3\Delta$ state is $|1^3\Delta\rangle \approx 0.82|1\sigma^2 2\sigma^2 3\sigma^1 1\pi_x^2 1\pi_y^2 1\delta_-^1\rangle$, whereas the $2^3\Delta$ and $^3\Gamma$ states are of intense multireference character with their largest configurations being $0.49|1\sigma^2 2\sigma^1 3\sigma^2 1\pi_x^2 1\pi_y^2 1\delta_-^1\rangle$ and $0.71|1\sigma^2 2\sigma^1 3\sigma^1 1\delta_+^1 1\pi_x^2 1\pi_y^2 1\bar{\delta}_-^1\rangle$, respectively.

Previous MRCI(+Q)/[$7s6p4d3f2g/_{Cr}5s4p3d2f1g/_C$] calculations[22] showed that the first excited state of CrC is a $^5\Sigma^-$ term with $T_e=9.2(9.6)$ kcal/mol, followed by a $^3\Delta$ term at $T_e=12.9(13.0)$ kcal/mol. Our present results locate the $1^3\Delta$ term at $T_e=7.91(13.3)$ kcal/mol, indicating that it could be the first excited state. Considering the largest basis set in conjunction with the state averaged approach employed here as compared to Ref. 22, the best we can say is that the $^5\Sigma^-$ and $1^3\Delta$ states are quasidegenerate.

D. Some general remarks

With the completion of this investigation, the group 6 diatomic carbides CrC, MoC,[50] and WC[51] are now all spectroscopically known. The CrC and MoC molecules are similar, both having $^3\Sigma^-$ ground states that are dominated by the $1\sigma^2 2\sigma^2 1\pi^4 1\delta^2$ configuration. This contrasts with the case of diatomic WC, where the ground state is $^3\Delta_1$, derived from the $1\sigma^2 2\sigma^2 3\sigma^1 1\pi^4 1\delta^1$ configuration. In CrC, this $^3\Delta$ state is a candidate for the first excited state (see Table III), calculated to lie 3000–5000 cm^{-1} above the ground state. The emergence of a different ground configuration for the 5*d*-metal carbide, as compared to the 3*d*- or 4*d*-metal carbides is turning out to be fairly common. For example, the ground states of the group 5 carbides, VC and NbC, are $^2\Delta_{3/2}$, arising from the $1\sigma^2 2\sigma^2 1\pi^4 1\delta^1$ configuration,[2,3,21,52] while recent, as yet unpublished, spectra from our laboratory demonstrate that the ground state of TaC is $^2\Sigma^+$, arising from the $1\sigma^2 2\sigma^2 3\sigma^1 1\pi^4$ configuration.[53] Similarly, the group 9 carbides, CoC and RhC, have ground states of $1\sigma^2 2\sigma^2 3\sigma^1 1\pi^4 1\delta^4$, $^2\Sigma^+$,[2,14,16,27,54–58] while the isovalent IrC molecule has a ground state of $1\sigma^2 2\sigma^2 3\sigma^2 1\pi^4 1\delta^3$, $^2\Delta_{5/2}$.[59–61] In all of these examples, the 3σ orbital, which is primarily metallic *ns* in character, is stabilized in the 5*d*-metal carbide due to the relativistic stabilization of the 6*s* orbital in the metal atom. The relativistic stabilization of the 6*s* orbital also

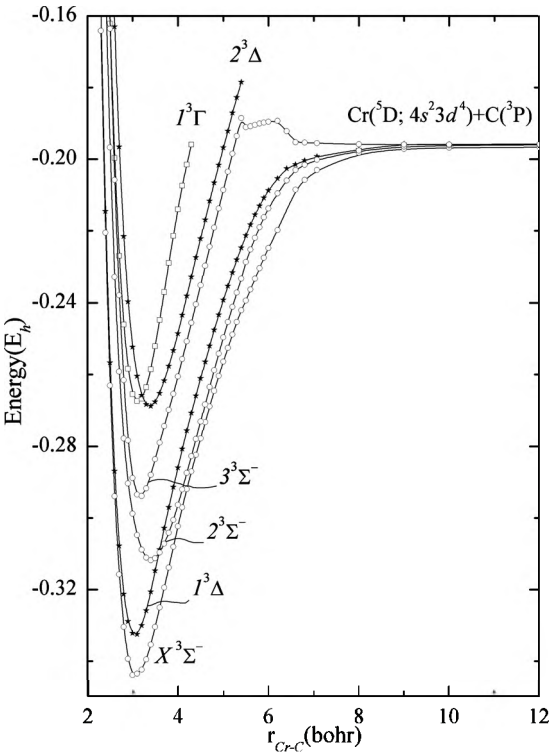

FIG. 4. MRCI/cc-pV5Z potential energy curves of the X $^3\Sigma^-$, $1^3\Delta$, 2 $^3\Sigma^-$, 3 $^3\Sigma^-$, $2^3\Delta$, and $1^3\Gamma$ states of CrC. All energies have been shifted by +1081.0E_h.

leads to a ground term for the tungsten atom of s^2d^4, ^{5}D, as opposed to the ground terms of s^1d^5, ^{7}S in Cr and Mo.[48] The relativistic stabilization of the 6*s*-based 3σ orbital causes it to be more readily occupied in the 5*d* metal carbides, as opposed to the 3*d*- and 4*d*-metal carbides. We expect this trend to continue as the ground states of additional 5*d* metal carbides are established.

Another observation about diatomic CrC that is quite striking is the size of its dipole moment, calculated here to be close to 6.8 D. To put this in perspective, diatomic LiF has a similar bond length as CrC (1.564 Å for LiF; 1.619 Å for CrC), and has a slightly smaller dipole moment of 6.328 ± 0.001 D in its ground vibronic level.[62] Compared to the other 3*d* transition metal carbides, the large dipole moment of CrC is anomalous. With the single exception of VC, all of the other 3*d* metal carbides have dipole moments below 3.5 D, as shown in Table IV. Further, the large dipole moments of VC and CrC do not result from a significantly larger amount of charge transfer to the carbon atom, as compared to the other metal carbides. In fact, ScC, TiC, and VC all have nearly the same Mulliken charges on the metal atom (+0.4), but the dipole moments are calculated to be 3.27, 1.53, and 7.36 D, respectively.[19–21] The large dipole moments of VC and CrC instead correlate to a lack of electron density in the metal 4*s*-based 3σ orbital, which is empty in the dominant configuration for these molecules. It is the lack of electron density in the highly polarizable 4*s* orbital that allows these two molecules to have such large dipole moments. In the other 3*d* carbides, the existence of a significant 4*s* electron density allows electrons to polarize away from the negatively charged carbon atom, creating a dipole moment that opposes the M^+C^- dipole. In effect, the charge distribution in the other metal carbides leads to a quadrupole moment along the z-axis, with a linear arrangement of charges, as $\delta^-\delta^+\delta^+\delta^-$. The large magnitude of the dipole moment in metal carbides that lack 3σ electrons has been verified in the case of MoC, which has the same electron configuration as CrC; in that case, the dipole moment has been measured to be 6.07 ± 0.18 D.[63]

V. SYNOPSIS

An electronic absorption band of CrC has been recorded, rotationally resolved, and analyzed for the first time. This demonstrates that the ground state is of $^3\Sigma^-$ symmetry with a bond length of $r_0 = 1.6188(6)$ Å, in agreement with *ab initio* calculations. The upper state is also of $^3\Sigma^-$ symmetry, with a bond length of $r' = 1.6861(5)$ Å. *Ab initio* MRCI studies demonstrate that the upper state is actually the third state of $^3\Sigma^-$ symmetry. Other computed properties of the lowest three $^3\Sigma^-$ terms, the lowest two $^3\Delta$ terms, and the lowest $^3\Gamma$ terms are also reported. Finally, comparisons are made to the other group 6 metal carbides, MoC and WC, and to the other 3*d* metal carbides. The relativistic stabilization of the 6*s* orbital in the 5*d* metal carbides is found to play a major role in reordering the molecular orbitals, and occupation of the 3σ orbital is calculated to dramatically reduce the dipole moment in all of the 3*d* transition metal carbides.

TABLE IV. Computed dipole moments of 3*d* transition metal carbides.

Molecule	Ground configuration, term	Mulliken charge on metal (CASSCF)	4*s* population	Calculated dipole (D)	Reference
ScC	$1\sigma^2 2\sigma^2 1\pi^3$, $^2\Pi$	+0.35	1.02	3.267	19
TiC	$1\sigma^2 2\sigma^1 3\sigma^1 1\pi^4$, $^3\Sigma^+$	+0.36	0.80	1.53	20
VC	$1\sigma^2 2\sigma^2 1\pi^4 1\delta^1$, $^2\Delta$	+0.38	0.29	7.36	21
CrC	$1\sigma^2 2\sigma^2 1\pi^4 1\delta^2$, $^3\Sigma^-$	+0.27	0.35	6.76	22 and present work
MnC	$1\sigma^2 2\sigma^2 3\sigma^1 1\pi^4 1\delta^2$, $^4\Sigma^-$	+0.30	0.84	2.35	23
FeC	$1\sigma^2 2\sigma^2 3\sigma^1 1\pi^4 1\delta^3$, $^3\Delta$	+0.31	0.84	1.94	24–26
CoC	$1\sigma^2 2\sigma^2 3\sigma^1 1\pi^4 1\delta^4$, $^2\Sigma^+$	+0.07	0.92	2.08	27
NiC	$1\sigma^2 2\sigma^2 3\sigma^2 1\pi^4 1\delta^4$, $^1\Sigma^+$	+0.19	1.12	2.25	28
CuC	$1\sigma^2 2\sigma^2 3\sigma^2 1\pi^4 1\delta^4 2\pi^1$, $^2\Pi$	+0.38	0.75	2.4	29

ACKNOWLEDGMENTS

D.J.B. and M.D.M. thank the U.S. Department of Energy for support of this research under Grant No. DE-FG03-01ER15176.

[1] J. F. Harrison, Chem. Rev. (Washington, D.C.) **100**, 679 (2000).
[2] R. J. Van Zee, J. J. Bianchini, and W. Weltner, Jr., Chem. Phys. Lett. **127**, 314 (1986).
[3] Y. M. Hamrick and W. Weltner, Jr., J. Chem. Phys. **94**, 3371 (1991).
[4] W. J. Balfour, J. Cao, C. V. V. Prasad, and C. X. Qian, J. Chem. Phys. **103**, 4046 (1995).
[5] M. D. Allen, T. C. Pesch, and L. M. Ziurys, Astrophys. J. **472**, L57 (1996).
[6] D. J. Brugh and M. D. Morse, J. Chem. Phys. **107**, 9772 (1997).
[7] K. Aiuchi, K. Tsuji, and K. Shibuya, Chem. Phys. Lett. **309**, 229 (1999).
[8] K. Aiuchi and K. Shibuya, J. Mol. Spectrosc. **209**, 92 (2001).
[9] M. Fujitake, A. Toba, M. Mori, F. Miyazawa, N. Ohashi, K. Aiuchi, and K. Shibuya, J. Mol. Spectrosc. **208**, 253 (2001).
[10] J. W. H. Leung, W. S. Tam, Q. Ran, and A. S. C. Cheung, Chem. Phys. Lett. **343**, 64 (2001).
[11] T. C. Steimle, W. L. Virgo, and D. A. Hostutler, J. Chem. Phys. **117**, 1511 (2002).
[12] P. M. Sheridan, L. M. Ziurys, and T. Hirano, Astrophys. J. **593**, L141 (2003).
[13] Y. C. Chang, C. S. Lam, B. Reed, K. C. Lau, H. T. Liou, and C. Y. Ng, J. Phys. Chem. A **113**, 4242 (2009).
[14] M. Barnes, A. J. Merer, and G. F. Metha, J. Chem. Phys. **103**, 8360 (1995).
[15] A. G. Adam and J. R. D. Peers, J. Mol. Spectrosc. **181**, 24 (1997).
[16] M. A. Brewster and L. M. Ziurys, Astrophys. J. **559**, L163 (2001).
[17] J.-R. Guo, Z.-X. Zhang, T.-T. Wang, C.-X. Chen, and Y. Chen, Chin. J. Chem. Phys. **21**, 505 (2008).
[18] D. J. Brugh and M. D. Morse, J. Chem. Phys. **117**, 10703 (2002).
[19] A. Kalemos, A. Mavridis, and J. F. Harrison, J. Phys. Chem. A **105**, 755 (2001).
[20] A. Kalemos and A. Mavridis, J. Phys. Chem. A **106**, 3905 (2002).
[21] A. Kalemos, T. H. Dunning, Jr., and A. Mavridis, J. Chem. Phys. **123**, 014301 (2005).
[22] A. Kalemos, T. H. Dunning, Jr., and A. Mavridis, J. Chem. Phys. **123**, 014302 (2005).
[23] A. Kalemos, T. H. Dunning, Jr., and A. Mavridis, J. Chem. Phys. **124**, 154308 (2006).
[24] D. Tzeli and A. Mavridis, J. Chem. Phys. **116**, 4901 (2002).
[25] D. Tzeli and A. Mavridis, J. Chem. Phys. **118**, 4984 (2003).
[26] D. Tzeli and A. Mavridis, J. Chem. Phys. **122**, 056101 (2005).
[27] D. Tzeli and A. Mavridis, J. Phys. Chem. A **110**, 8952 (2006).
[28] D. Tzeli and A. Mavridis, J. Chem. Phys. **126**, 194304 (2007).
[29] A. Kalemos, T. H. Dunning, Jr., and A. Mavridis, J. Chem. Phys. **129**, 174306 (2008).
[30] I. S. K. Kerkines, J. Pittner, P. Carsky, A. Mavridis, and I. Hubac, J. Chem. Phys. **117**, 9733 (2002).
[31] A. Tsouloucha, I. S. K. Kerkines, and A. Mavridis, J. Phys. Chem. A **107**, 6062 (2003).
[32] W. C. Wiley and I. H. McLaren, Rev. Sci. Instrum. **26**, 1150 (1955).
[33] B. A. Mamyrin, V. I. Karataev, D. V. Shmikk, and V. A. Zagulin, Zh. Eksp. Teor. Fiz. **64**, 82 (1973).
[34] P. R. Bevington, *Data Reduction and Error Analysis for the Physical Sciences* (McGraw-Hill, New York, 1969).
[35] G. A. Bishea, J. C. Pinegar, and M. D. Morse, J. Chem. Phys. **95**, 5630 (1991).
[36] J. M. Behm, C. A. Arrington, J. D. Langenberg, and M. D. Morse, J. Chem. Phys. **99**, 6394 (1993).
[37] S. Gerstenkorn and P. Luc, *Atlas du Spectre d'Absorption de la Molécule d'Iode Entre* 14,800–20,000 cm^{-1} (CNRS, Paris, 1978).
[38] S. Gerstenkorn and P. Luc, Rev. Phys. Appl. (Paris) **14**, 791 (1979).
[39] N. B. Balabanov and K. A. Peterson, J. Chem. Phys. **123**, 064107 (2005).
[40] T. H. Dunning, Jr., J. Chem. Phys. **90**, 1007 (1989).
[41] H.-J. Werner, P. J. Knowles, R. Lindh *et al.*, MOLPRO, version 2009.1, a package of *ab initio* programs, see http://www.molpro.net.
[42] S. R. Langhoff and E. R. Davidson, Int. J. Quantum Chem. **8**, 61 (1974).
[43] E. R. Davidson and D. W. Silver, Chem. Phys. Lett. **52**, 403 (1977).
[44] H. Lefebvre-Brion and R. W. Field, *The Spectra and Dynamics of Diatomic Molecules* (Elsevier, Amsterdam, 2004).
[45] E. Ishiguro and M. Kobori, J. Phys. Soc. Jpn. **22**, 263 (1967).
[46] C. M. Western, PGOPHER, a program for simulating rotational structure, University of Bristol, http://pgopher.chm.bris.ac.uk.
[47] G. Herzberg, in *Molecular Spectra and Molecular Structure I. Spectra of Diatomic Molecules*, 2nd ed. (Van Nostrand Reinhold, New York, 1950).
[48] C. E. Moore, *Atomic Energy Levels*, Natl. Bur. Stand. U.S. Circ. No. 467 ed. (U.S. Government Printing Office, Washington, D. C., 1971).
[49] I. S. K. Kerkines and A. Mavridis, Mol. Phys. **102**, 2451 (2004).
[50] D. J. Brugh, T. J. Ronningen, and M. D. Morse, J. Chem. Phys. **109**, 7851 (1998).
[51] S. M. Sickafoose, A. W. Smith, and M. D. Morse, J. Chem. Phys. **116**, 993 (2002).
[52] B. Simard, P. I. Presunka, H. P. Loock, A. Bérces, and O. Launila, J. Chem. Phys. **107**, 307 (1997).
[53] O. Krechkivska and M. D. Morse, "Resonant two-photon ionization spectroscopy of jet-cooled tantalum carbide, TaC," J. Chem. Phys. (in press).
[54] A. Lagerqvist and R. Scullman, Ark. Fys. **32**, 475 (1966).
[55] B. Kaving and R. Scullman, J. Mol. Spectrosc. **32**, 475 (1969).
[56] J. M. Brom, Jr., W. R. M. Graham, and W. Weltner, Jr., J. Chem. Phys. **57**, 4116 (1972).
[57] H. Tan, M. Liao, and K. Balasubramanian, Chem. Phys. Lett. **280**, 423 (1997).
[58] W. J. Balfour, S. G. Fougère, R. F. Heuff, C. X. W. Qian, and C. Zhou, J. Mol. Spectrosc. **198**, 393 (1999).
[59] K. Jansson and R. Scullman, J. Mol. Spectrosc. **36**, 248 (1970).
[60] H. Tan, M. Liao, and K. Balasubramanian, Chem. Phys. Lett. **280**, 219 (1997).
[61] T. Ma, J. W. H. Leung, and A. S. C. Cheung, Chem. Phys. Lett. **385**, 259 (2004).
[62] L. Wharton, W. Klemperer, L. P. Gold, R. Strauch, J. J. Gallagher, and V. E. Derr, J. Chem. Phys. **38**, 1203 (1963).
[63] H. Wang, W. L. Virgo, J. Chen, and T. C. Steimle, J. Chem. Phys. **127**, 124302 (2007).